Noninvasive Imaging of Human Telomerase Reverse Transcriptase (hTERT) Messenger RNA with ^{99m}Tc-Radiolabeled Antisense Probes in Malignant Tumors

Meng Liu, Rong Fu Wang, Chun Li Zhang, Ping Yan, Ming Ming Yu, Li Juan Di, Hong Jie Liu, and Feng Qin Guo

Department of Nuclear Medicine, Peking University First Hospital, West District, Beijing, China

The expression of human telomerase reverse transcriptase (hTERT) is present in most malignant cells (>85%) but is undetectable in most normal somatic cells. Visualization of hTERT expression using radionuclide targeting can provide important diagnostic information in malignant tumors. The overall aim of this study was to evaluate whether ^{99m}Tc-radiolabeled antisense oligonucleotide (ASON) targeting hTERT messenger RNA (mRNA) can be used for imaging of hTERT expression in vivo. **Methods:** One 18-mer antisense or sense uniformly phosphorothioate-modified oligonucleotide targeting hTERT mRNA was radiolabeled with ^{99m}Tc through the bifunctional chelator *N*-hydroxysuccinimidyl derivative of *S*-acetylmercaptoacetyltriglycine (*S*-acetyl NHS-MAG3). Then the radiolabeled probe was characterized in vitro. Reverse transcription-polymerase chain reaction (RT-PCR) was performed to assay the mRNA level after proliferating cells had been incubated with the antisense and sense probes. ^{99m}Tc-MAG3-ASON or ^{99m}Tc-MAG3-SON was injected intravenously in mammary tumor-bearing BALB/c nude mice. Biodistribution and in vivo imaging was performed periodically. All data were analyzed by statistical software. **Results:** The labeling efficiencies of ^{99m}Tc-MAG3-ASON/SON reached 76% ± 5% ($n = 5$) within 15–30 min at room temperature, the specific activity was up to 1,850 kBq/μg, and the radiochemical purity was >96% after purification. ^{99m}Tc-MAG3-ASON showed complete stability at room temperature and in fresh 37°C human serum. In comparison with ^{99m}Tc-MAG3-SON, ^{99m}Tc-MAG3-ASON preserved the capacity to bind living hTERT-expressing cells specifically and to inhibit the expression of hTERT mRNA significantly as well as ASON. In nude mice bearing hTERT-expressing MCF-7 xenografts, tumor radioactivity uptake of ^{99m}Tc-MAG3-ASON after injection was significantly higher than that of ^{99m}Tc-MAG3-SON after injection ($P < 0.05$). The hTERT-expressing xenografts were clearly imaged at 4–8 h noninvasively after injection of ^{99m}Tc-MAG3-ASON, whereas the xenografts were not imaged at any time after injection of ^{99m}Tc-MAG3-SON. **Conclusion:** This in vivo study provides evidence that ^{99m}Tc-MAG3-ASON targeting hTERT mRNA can be used as a potential candidate for visualization of hTERT expression in carcinomas.

Key Words: ^{99m}Tc; antisense; molecular imaging; human telomerase reverse transcriptase; hTERT; biodistribution

J Nucl Med 2007; 48:2028–2036
DOI: 10.2967/jnumed.107.042622

Telomerase, a hallmark of malignant tumors, is minimally composed of the telomerase RNA (hTR), the telomerase reverse transcriptase (hTERT), and telomerase-associated proteins (*1,2*). hTERT represents the major determinant of telomerase activity. In contrast to hTR, which is commonly expressed in both normal tissues (without telomerase activity) and cancers, hTERT expression is found solely in tumor cells. Consequently, hTERT is one of the most attractive molecular markers available, promising a target spectrum of approximately 85% of all tumors (*3,4*). In addition, hTERT expression enhances the chemoresistance of cancer cells, and effective therapies are associated with decreased expression of hTERT, so imaging of hTERT expression also has prognostic value (*5,6*).

Although it has potential clinical significance, the measurement of hTERT expression has predominantly been by immunohistochemistry or by reverse transcription-polymerase chain reaction (RT-PCR), which requires the destruction of the tissues or cells examined. At present, reporter genes have provided new methods for noninvasive imaging, combining molecular biology with techniques such as fluorescent imaging, bioluminescent imaging, and radionuclide imaging. This indirect imaging paradigm usually includes a "marker/reporter gene", a "marker/reporter probe," and imaging technology that can visualize the spatial distribution of a probe (*7,8*). Examples using radionuclide or trimodality fusion imaging of hTERT promoter activity were recently published, and the results were encouraging (*9,10*).

However, direct inhibition of telomerase activity in cancer cells, a significant strategy, has been proposed. Compared with indirect imaging, imaging endogenous expression

Received Apr. 9, 2007; revision accepted Sep. 10, 2007.
For correspondence or reprints contact: Rong Fu Wang, MD, PhD, Department of Nuclear Medicine, Peking University First Hospital, No. 8, Xishiku St., West District, Beijing, 100034, China.
E-mail: rongfu_wang2003@yahoo.com.cn

directly is more important, despite its greater difficulty, because it is directed at the genotypic basis of the normal phenotypic function of cells and at the alterations at gene expression that can initiate disease (*11*). Thus, antisense imaging is one of the most promising tools of molecular imaging, whose strategies exploit the exquisite specificity of nucleic acid base-pair binding. Although there is much controversy, the use of antisense imaging as an in vivo diagnostic method is still attractive in that it would bring molecular imaging to the level of gene expression, especially for the early detection of tumor.

In present study, we tried to use antisense oligonucleotide (ASON) to noninvasively measure hTERT messenger RNA (mRNA) expression directly. One 18-mer antisense uniformly phosphorothioate-modified oligonucleotide targeting hTERT mRNA was radiolabeled with ^{99m}Tc. We evaluated the characteristics of this antisense probe in vitro and observed whether it could be used for imaging of hTERT expression in malignant tumors in vivo.

MATERIALS AND METHODS

All oligonucleotides were purchased from the same source as the uniform phosphorothioates (Sangon Biotechnologies), purified with polyacrylamide gel electrophoresis (PAGE), and used as supplied. The sequence of ASON is 5′-TAGAGACGTGGCTCT-TGA-3′, and that of sense oligonucleotide (SON) is 5′-TCAAG-AGCCACGTCTCTA-3′, both with a primary amine on the terminal 3′ phosphate group via a 6-member methylene carbon spacer, which was designed for covalent conjugation with the chelator. The molecular weight of chain was about 5.5 kDa each. The amine ASON/SON was generally handled under sterile conditions. The chelator of the *N*-hydroxysuccinimidyl derivative of *S*-acetylmercaptoacetyltriglycine (*S*-acetyl NHS-MAG3) was kindly provided by Donald J. Hnatowich (University of Massachusetts Medical School). Sephadex G25 (Amersham) was purchased and used as received. All other chemicals were reagent grade and were used without purification. The fresh ^{99m}Tc-pertechnetate generator eluate was obtained from a ^{99}Mo-^{99m}Tc radionuclide generator (China Institute of Atomic Energy).

Oligonucleotide Conjugation and Radiolabeling

ASON with a primary amine on the terminal 3′ phosphate group was conjugated with *S*-acetyl NHS-MAG3 as described (*12,13*). In brief, a solution of ASON was prepared at a concentration of 5 μg/μL in 0.1 M *N*-(2-hydroxyethyl)piperazine-*N*′-(2-ethanesulfonic acid) (HEPES) buffer, pH 8.0. A fresh 20 mg/mL solution of *S*-acetyl-NHS-MAG3 in dry *N,N*-dimethylformamide (DMF) was added dropwise with agitation to a final MAG3-to-ASON molar ratio of 20:1. This reaction mixture was incubated at room temperature for 60–120 min. Then the conjugated ASON was purified on a 0.7 × 20 cm Sephadex G25 gel-filtration column using sterile 50 mM phosphate buffer, pH 7.2, as eluant. The peak fractions were pooled, and the DNA concentration was quantitated by a recording ultraviolet visible spectrophotometer (SMA3000; Beijing Genomics Institute, China) at 260 nm (optical density, 33 μg/mL). The preparation of MAG3-ASON was dispensed at 10 μg per vial, lyophilized, and stored at −20°C for future use. SON was treated as described for ASON.

A fresh 50 mg/mL solution of sodium tartrate was prepared in sterile 0.5 M sodium bicarbonate, 0.25 M ammonium acetate, 0.175 M ammonium hydroxide, pH 9.2. The high pH of the tartrate solution was necessary so that the final pH would be approximately 7.6. In addition, a 1 mg/mL solution of $SnCl_2{\cdot}2H_2O$ in 10 mM hydrochloric acid was prepared just before use. At room temperature, the conjugated and purified MAG3-ASON (10 μg) was typically dissolved at a concentration of 500 μg/mL in 0.25 M ammonium acetate buffer, pH 5.2. To the solution of MAG3-ASON, sodium tartrate was added as a transchelator to a final concentration of about 7 μg/μL, and the labeling pH reached 7.6. Then sufficient ^{99m}Tc-pertechnetate generator eluate (10 μL) was added to this solution to provide about 3,700 kBq/μg of ASON. The stannous ion solution was added immediately thereafter such that 1 μg of $SnCl_2{\cdot}2H_2O$ was added for each 10 μg of ASON. After 15–30 min, the labeled MAG3-ASON preparation was purified on a 0.7 × 20 cm Sephadex G25 gel-filtration column with 50 mM phosphate buffer, pH 7.2, eluant. Fractions were collected to detect the radioactivity and absorbance at 260 nm. SON was radiolabeled identically with ^{99m}Tc.

For routine quality control of labeling, the labeling efficiency and radiochemical purity of radiolabeled probes were calculated by paper chromatography on Xinhua no. 1 filter paper with acetone and normal saline as the mobile phase.

In Vitro Stability Analysis

To evaluate the labeling stability, the radiochemical purity of ^{99m}Tc-MAG3-ASON at room temperature, as well as that in normal saline at room temperature and in fresh 37°C human serum at 0.01 μg/μL, was confirmed by paper chromatography periodically over 24 h.

PAGE was performed to assess the stability of ^{99m}Tc-MAG3-ASON in serum by comparing the electrophoretic mobility. Incubation with fresh 37°C human serum for 1, 2, 4, and 6 h later, ^{99m}Tc-MAG3-ASON was extracted by a phenol/chloroform method. After ethanol precipitation at −20°C overnight, the samples were centrifugated (12,000*g*/min) for 10 min. The precipitation was dried naturally and redissolved in distilled water. Then the samples in each time point, including the control, were resolved on 20% PAGE and stained with silver nitrate. The resulting gels were finally scanned using an ultraviolet transilluminator (AlphaImager 2200; Alpha Innotech Corp.) and photographed.

Cell Culture

The HepG2 cell line was a generous gift from the Department of Infectious Disease, Peking University First Hospital, and was maintained in the media recommended by them. The cells were grown in Dulbecco's modified Eagle medium (DMEM) containing L-glutamine (2 mM), sodium bicarbonate (1.5 mg/L), nonessential amino acids (0.1 mM), and sodium pyruvate (1.2 mM), supplemented with 10% fetal bovine serum (FBS) and 100 mg/mL of penicillin–streptomycin (GIBCO). Cells were cultivated under standard conditions (37°C, humidified atmosphere containing 5% CO_2). Cells between passages 4 and 12 were used and were harvested by trypsin treatment (0.25% trypsin/0.02% ethylenediaminetetraacetic acid, 5 min, 37°C). The cell growth status was monitored by inverted microscopy with phase contrast, and cell viability was assessed by trypan blue exclusion.

Cell Transfections

Before transfection, the cells were seeded in appropriate culture plates and grown for 2 d. On the third day, the cells were

transfected once, with a mixture consisting of molecular probe and liposome (ratio, 1:3 w/w, diluted in serum-free OptiMEM) according to the manufacturer's instructions (Lipofectamine 2000; Invitrogen). After incubation under standard conditions for 4 h, the cells were washed with phosphate-buffered saline (PBS) and incubated in fresh culture medium (DMEM with 10% FBS) to maintain growth, until additional analyses.

RT-PCR

After transfection with ^{99m}Tc-MAG3-ASON, ^{99m}Tc-MAG3-SON, and ASON, respectively, the cells were trypsinized and washed twice with PBS. The total cellular RNA was extracted from the HepG2 cells by Trizol 1-step method (TRIZOL reagent; Bio Basic Inc.). For reverse transcription, 2 μg of total RNA were subjected to reverse transcription primed by oligodeoxythymidine with avian myeloblastosis virus reverse transcriptase according to the recommendations of the First Strand cDNA Synthesis Kit (Bio Basic Inc.). Then the complementary DNA (cDNA) was applied to perform PCR using the PCR Kit (Sangon Biotechnologies). As an internal control for cDNA synthesis, the housekeeping gene of β-actin was amplified too. PCR primers were as follows:

hTERT: (left primer)
5′-TCTACCGGAAGAGTGTCTGGAGCAA-3′
(right primer) 5′-GCTCCCACGACGTAGTCCATGTTCA-3′
202-bp predicted product size.

β-Actin: (left primer) 5′-GTGGGGCGCCCCAGGCACCA-3′
(right primer) 5′-GTCCTTAATGTCACGCACGATTTC-3′
540-bp predicted product size.

PCR amplification of hTERT cDNA was performed with an initial heating at 94°C for 4 min, followed by 34 cycles consisting of denaturing for 30 s at 94°C, annealing for 30 s at 61°C, and elongation for 30 s at 72°C, and a final extension period of 5 min at 72°C. PCR amplification of β-actin was performed as described. Amplified products were size-fractionated by 2% agarose gel electrophoresis. The gel was stained with ethidium bromide (1 μg/mL), visualized by an ultraviolet transilluminator, and photographed. The density of each PCR band was measured and analyzed by video documentation system software (AlphaImager version 5.5; Alpha Innotech Corp.). The amount of mRNA products for hTERT was expressed as the ratio to β-actin mRNA product, which was conserved as the internal control.

Biodistribution of ^{99m}Tc-MAG3-ASON and ^{99m}Tc-MAG3-SON in MCF-7 Xenograft-Bearing Nude Mice After Systemic Injection

BALB/c *nu/nu* mice (female, 20 ± 3 g, 4- to 6-wk-old; Department of Laboratory Animal Science, Peking University Health Science Center) were used in this study. The mice were inoculated with 1×10^7 MCF-7 mammary tumor cells (obtained from Department of Laboratory Animal Science, Peking University Health Science Center) in the right upper limbs, and the tumors were allowed to grow to a diameter of 1.0 cm. The mice were maintained using a standard diet, bedding, and environment, with free access to food and drinking water.

Fifty BALB/c *nu/nu* mice with MCF-7 xenografts were randomly divided into 10 groups of 5 mice each (5 groups for injection of antisense probe, another 5 groups for injection of sense probe). Immediately after Sephadex G25 gel-filtration column purification, 1 μg (1,850 kBq) of ^{99m}Tc-MAG3-ASON (or ^{99m}Tc-MAG3-SON) in 100 μL of eluant (50 mM phosphate buffer, pH 7.2) was injected into each mouse via a tail vein. All injections were tolerated well. At 0.5, 1, 2, 4, and 6 h after injection, the mice were sacrificed by cervical dislocation. Then the mice were dissected and tissues of interest (heart, liver, spleen, lung, kidney, stomach, small intestine, bladder, skeletal muscle, bone marrow, blood, and tumor) were weighed, and their radioactivity was measured using a γ-well counter along with a standard of the injection. Radioactivity results were recorded as the percentage injected activity per gram (%ID/g) of tissue corrected for background and decay.

γ-Camera Imaging

Ten BALB/c *nu/nu* mice with MCF-7 xenografts were randomly divided into 2 groups of 5 mice each (one group for injection of antisense probe, the other for injection of sense probe). Immediately after Sephadex G25 gel-filtration column purification, 4 μg (7,400 kBq) of the antisense or sense probe in 100 μL of eluant (50 mM phosphate buffer, pH 7.2) were injected into each mouse via a tail vein. All injections were tolerated well. At 0.5, 1, 2, 4, 6, and 8 h after injection, imaging was performed in the Department of Nuclear Medicine, Peking University First Hospital, using SPECT (SPR SPECT; GE Healthcare, Inc.) equipped with a low-energy, high-resolution, parallel-hole collimator. Static images (100,000 counts), obtained with a zoom factor of 2.0, were digitally stored in a 256 × 256 matrix.

Statistical Analysis

The variables are expressed as average ± SD ($\bar{\chi}$ ± SD). The variables of RT-PCR were analyzed using 1-way ANOVA, and other statistical comparisons of average values were performed with the Student t test. $P < 0.05$ was considered significant.

RESULTS

Oligonucleotide Conjugation and Radiolabeling

Under the set of conditions, average labeling efficiencies of 76% ± 5% ($n = 5$) were achieved within 15–30 min at room temperature, specific activities of up to 1,850 kBq/μg were obtained, and radiochemical purity was >96% after purification. Control labeling of unmodified ASON under the same conditions showed only about 5% ± 1.6% ($n = 5$) binding, indicating that radiolabeling was largely specific and mediated by the chelator.

The labeling efficiency and radiochemical purity of radiolabeled agent were calculated by the paper chromatography on Xinhua no. 1 filter paper with acetone and normal saline as the mobile phase. With acetone as the mobile phase, only ^{99m}Tc-pertechnetate migrated with the solvent, whereas ^{99m}Tc-MAG3-ASON and other labeled colloids remained at the origin. Otherwise, with the normal saline as the mobile phase, ^{99m}Tc-pertechnetate and ^{99m}Tc-MAG3-ASON migrated with the solvent, whereas labeled colloids remained at the origin (Table 1).

In Vitro Stability Analysis

The radiochemical purity of ^{99m}Tc-MAG3-ASON under different conditions was >93% periodically over 24 h (Fig. 1).

TABLE 1
R_f Value in 2 Kinds of Developing Solvents

Developing solvent	R_f value		
	$^{99m}TcO_4^-$	^{99m}Tc-MAG3-ASON	$^{99m}TcO_2$
Acetone	0.9–1.0	0–0.1	0–0.1
Normal saline	0.9–1.0	0.8–1.0	0–0.1

It is very important for radiolabeled ASON to retain stability when considered for the application in imaging in vivo. PAGE can differentiate even 1 base change of oligonucleotide, so it is a highly sensitive method for detecting the probability of degradation of ASON. PAGE showed that radiolabeled probe remained stable in fresh 37°C human serum (Fig. 2).

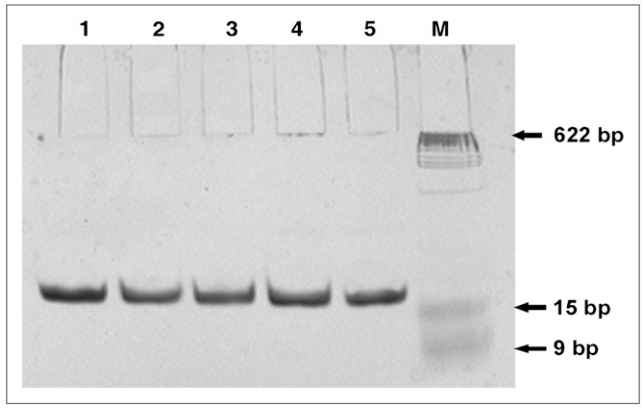

FIGURE 2. Stability of ^{99m}Tc-MAG3-ASON in fresh 37°C human serum. Lane M, DNA standard marker; lane 1, control group without incubation; lanes 2, 3, 4, and 5, groups incubated with fresh 37°C human serum for 1, 2, 4, and 6 h, respectively. PAGE shows that there is only 1 band in the same position, indicating the nondegradation of ^{99m}Tc-MAG3-ASON by the nuclease in serum. bp = base pairs.

RT-PCR

A significant decrease of hTERT mRNA expression was observed in cells treated with ^{99m}Tc-MAG3-ASON and ASON compared with that in cells treated with ^{99m}Tc-MAG3-SON and 10% FBS ($P < 0.05$, $n = 3$). However, there were no significant differences of hTERT mRNA expression between the cells treated with ^{99m}Tc-MAG3-SON and 10% FBS and between the cells treated with ^{99m}Tc-MAG3-ASON and ASON (Fig. 3).

Biodistribution of ^{99m}Tc-MAG3-ASON and ^{99m}Tc-MAG3-SON in MCF-7 Xenograft-Bearing Nude Mice After Systemic Injection

Biodistribution data are shown in Tables 2 and 3. At a different time phase after injection of ^{99m}Tc-MAG3-ASON, the probe accumulated primarily in the kidney and liver, followed by the stomach and tumor. None of the other organs (and tissues) investigated showed high uptake of radiolabeled ASON. A high renal radioactivity accumulation indicated that the substance was cleared primarily through the urinary system. In addition, the biodistribution of ^{99m}Tc-MAG3-ASON was characterized by quick blood clearance, with 2.62 ± 0.167 %ID/g remaining 0.5 h after injection and 1.051 ± 0.121 %ID/g remaining at 2 h. The biodistribution of ^{99m}Tc-MAG3-SON shared similar characteristics with ^{99m}Tc-MAG3-ASON, except the radioactivity uptake in tumor.

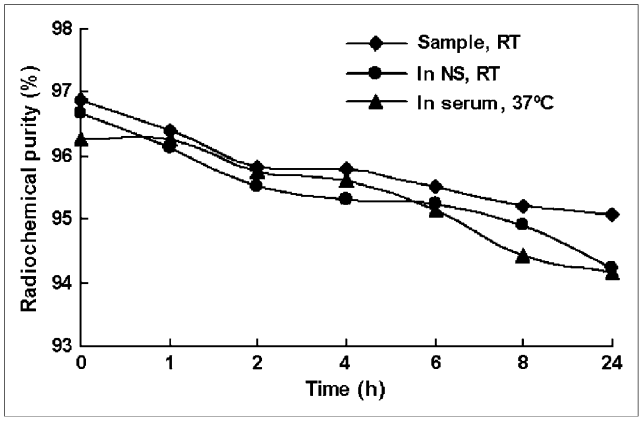

FIGURE 1. Radiochemical purity of ^{99m}Tc-MAG3-ASON at room temperature (RT), in normal saline (NS) at RT, and in fresh 37°C human serum at 0.01 μg/μL always remains >93% periodically over 24 h.

In comparison with radioactivity concentration in the tumor after injection of ^{99m}Tc-MAG3-ASON, that after injection of ^{99m}Tc-MAG3-SON was significantly lower ($P < 0.05$) (Fig. 4). Due to blood clearance, the tumor uptake of ^{99m}Tc-MAG3-SON was gradually decreasing. However, the tumor uptake of ^{99m}Tc-MAG3-ASON increased after 2 h and remained at the relatively high level until the 6-h time point after injection. As a result, the tumor-to-nontumor (T/NT) accumulation ratio after injection of ^{99m}Tc-MAG3-ASON was significantly higher than that after injection of ^{99m}Tc-MAG3-SON, especially after 4 h (Fig. 5). After injection of ^{99m}Tc-MAG3-ASON, the tumor-to-muscle (T/M) ratio exceeded 8.8, and the tumor-to-blood (T/B) ratio reached 2.0 at 6 h.

γ-Camera Imaging

In nude mice bearing hTERT-expressing MCF-7 xenografts, the tumors were clearly imaged at 4–8 h noninvasively after the administration of ^{99m}Tc-MAG3-ASON. On the contrary, the tumors were not imaged at any time after injection of ^{99m}Tc-MAG3-SON (Fig. 6). As predicted from the biodistribution studies, the renal route of elimination of the probes also led to substantial radioactivity accumulation in the abdomen.

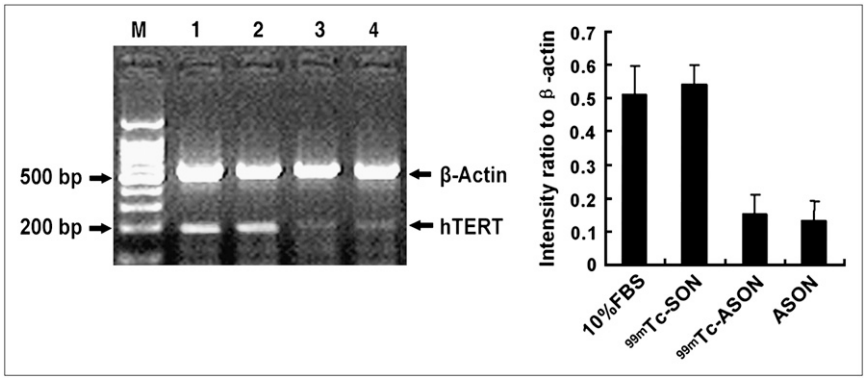

FIGURE 3. Effect of ^{99m}Tc-MAG3-ASON, ^{99m}Tc-MAG3-SON, and ASON on hTERT mRNA expression. Lane M, DNA standard marker; lane 1, cells incubated with 10% FBS; lane 2, cells treated with ^{99m}Tc-MAG3-SON; lane 3, cells treated with ^{99m}Tc-MAG3-ASON; lane 4, cells treated with ASON. Intensity ratio of each band to internal control (β-actin) shows significantly lower quantity of hTERT mRNA ($P < 0.05$) in cells treated with ^{99m}Tc-MAG3-ASON and ASON compared with that in cells treated with ^{99m}Tc-MAG3-SON and 10% FBS. bp = base pairs.

DISCUSSION

The induction of hTERT expression results in telomerase activity and contributes, as part of a multistep process, to human carcinogenesis. Most malignant tumors (>85%) show hTERT activity. Therefore, targeting the catalytic subunit hTERT represents a promising approach for providing diagnostic value in several types of cancer, and it will probably not cause substantial side effects on telomerase-negative, somatic cells (*14–16*). Until recently, the measurement of hTERT expression required the destruction of the tissues or cells under investigation, such as immunohistochemistry or PCR. There are also some reports about nondestructive methods of measuring hTERT expression using reporter gene imaging, in which hTERT serves as a promoter. Because the detection of hTERT expression has potential clinical significance, we attempt to use antisense imaging to measure hTERT expression in vivo directly.

Antisense imaging, a specific and noninvasive technology, is based on the complementarity of the constructs to the appropriate target mRNA. Pioneering work in this field was reported by Dewanjee MK et al. in 1994, who used a 15-mer phosphorothioate antisense oligodeoxyribonucleotide labeled with ^{111}In to image constitutive c-myc gene expression in a murine mammary carcinoma model (*17*). Up to now, ASONs targeting c-MYC, P-glycoprotein (Pgp), CCND1, mdr1, bcl-2, k-ras, unr, IgV_H FR1 mRNA, and so forth have been chosen to be labeled with radionuclides such as ^{99m}Tc, ^{111}In, ^{68}Ga, ^{64}Cu, ^{131}I and so forth (*18–26*), whose results all facilitate the development of antisense imaging. Despite an extensive literature search, we failed to find any research publication describing in vivo imaging of hTERT expression by antisense technology. In the present study, we used radiolabeled ASON targeting hTERT mRNA to measure hTERT expression in malignant tumors in vivo.

The choice of an efficient ASON targeting hTERT mRNA is critical. One of the limiting factors, discriminating between efficient and ineffective ASONs, is the accessibility of the target RNA sequence, because stable secondary structures might prevent ASON hybridization. Experimental ("walk the gene," ribonuclease H mapping), as well as theoretic, procedures (secondary structure prediction of the RNA) should increase the probability of finding effective antisense molecules (*27,28*). Another key factor is the optimum length that the ASON needs to bind to its target. According to statistical calculations, the

TABLE 2
Biodistribution (%ID/g) of ^{99m}Tc-MAG3-ASON in Mice Bearing MCF-7 Xenografts

Biodistribution	0.5 h	1 h	2 h	4 h	6 h
Heart	1.183 ± 0.232	0.889 ± 0.142	0.433 ± 0.11	0.465 ± 0.1	0.42 ± 0.072
Liver	4.167 ± 0.476	2.29 ± 0.227	2.613 ± 0.297	2.1 ± 0.275	2.15 ± 0.283
Spleen	1.417 ± 0.183	0.788 ± 0.085	0.549 ± 0.034	0.527 ± 0.086	0.516 ± 0.088
Lung	3.213 ± 0.154	2.47 ± 0.188	1.066 ± 0.12	0.906 ± 0.054	0.98 ± 0.188
Kidney	13.27 ± 1.99	8.16 ± 1.88	5.889 ± 0.953	5.39 ± 0.808	4.717 ± 1.767
Stomach	2.59 ± 0.166	1.89 ± 0.211	1.855 ± 0.248	1.72 ± 0.06	1.19 ± 0.016
Small intestine	2.39 ± 0.9	1.71 ± 0.764	0.902 ± 0.14	0.646 ± 0.029	0.538 ± 0.19
Bladder	1.581 ± 0.371	1.992 ± 0.947	0.92 ± 0.264	0.526 ± 0.136	0.329 ± 0.219
Skeletal muscle	0.556 ± 0.035	0.344 ± 0.022	0.22 ± 0.024	0.143 ± 0.028	0.165 ± 0.031
Bone marrow	1.227 ± 0.14	1.27 ± 0.158	0.766 ± 0.128	0.548 ± 0.078	0.59 ± 0.132
Blood	2.62 ± 0.167	1.5 ± 0.147	1.051 ± 0.121	0.912 ± 0.177	0.772 ± 0.107
Tumor	2.039 ± 0.136	1.5 ± 0.168	1.07 ± 0.137	1.157 ± 0.182	1.46 ± 0.178

Each value represents average of 5 mice ± SD and is expressed as %ID radioactivity per gram organ or tissue.

TABLE 3
Biodistribution (%ID/g) of ^{99m}Tc-MAG3-SON in Mice Bearing MCF-7 Xenografts

Biodistribution	0.5 h	1 h	2 h	4 h	6 h
Heart	0.606 ± 0.173	0.488 ± 0.083	0.358 ± 0.057	0.313 ± 0.097	0.454 ± 0.121
Liver	2.74 ± 0.254	2.26 ± 0.221	2.287 ± 0.298	1.93 ± 0.177	1.954 ± 0.123
Spleen	0.939 ± 0.033	0.595 ± 0.065	0.52 ± 0.032	0.448 ± 0.076	0.415 ± 0.054
Lung	2.01 ± 0.144	1.68 ± 0.132	0.883 ± 0.146	0.854 ± 0.189	0.841 ± 0.032
Kidney	9.218 ± 0.78	6.74 ± 1.08	4.94 ± 0.549	4.38 ± 1.07	3.23 ± 0.477
Stomach	2.42 ± 0.191	1.55 ± 0.155	1.62 ± 0.147	1.61 ± 0.185	1.17 ± 0.184
Small intestine	1.505 ± 0.162	1.982 ± 0.183	1.1 ± 0.08	0.427 ± 0.085	0.259 ± 0.049
Bladder	1.909 ± 0.162	1.474 ± 0.124	0.987 ± 0.123	0.365 ± 0.097	0.309 ± 0.168
Skeletal muscle	0.523 ± 0.036	0.297 ± 0.025	0.232 ± 0.035	0.239 ± 0.053	0.211 ± 0.021
Bone marrow	1.22 ± 0.155	0.707 ± 0.099	0.497 ± 0.121	0.554 ± 0.163	0.328 ± 0.11
Blood	1.78 ± 0.173	1.67 ± 0.134	0.947 ± 0.163	0.779 ± 0.12	0.476 ± 0.056
Tumor	0.772 ± 0.082	0.663 ± 0.127	0.59 ± 0.095	0.503 ± 0.051	0.417 ± 0.09

Each value represents average of 5 mice ± SD and is expressed as %ID radioactivity per gram organ or tissue.

optimum size should be between 15 and 20 bases for a given oligonucleotide to meet only 1 target in the human genome (*29*). On the basis of the principles of ASON design and previous study (*30*), the ASON of 5′-TAGAGACGT-GGCTCTTGA-3′, which is complementary to the hTERT mRNA (4,015 nucleotides; accession no. AF015950), was chosen. BLAST (Basic Local Alignment Search Tool) database searches performed for ASON revealed no complementary sequences to mRNAs (except for hTERT mRNA).

Considering several important reasons—such as the good imaging characteristics, facile logistics of delivery, well-studied labeling chemistry, ready availability, and even potentially clinical practice—we directed our efforts toward developing a ^{99m}Tc-labeled probe for single-photon detection. Because ^{99m}Tc is a γ-emitting metal, radiolabeling is usually accomplished by chelation to exogenous chelators previously conjugated to the oligonucleotides. As a result, the labeling efficiency of ^{99m}Tc-labeled MAG3-ASON/SON was >75%, the radiochemistry purity after purification was up to 96%, and the specific activities were 1,850 kBq/μg. In addition, ^{99m}Tc-MAG3-ASON showed stability and completeness at room temperature and in fresh 37°C human serum. These characteristics of ^{99m}Tc-MAG3-ASON showed that this radiolabeled probe was suitable for the purpose of imaging in vivo.

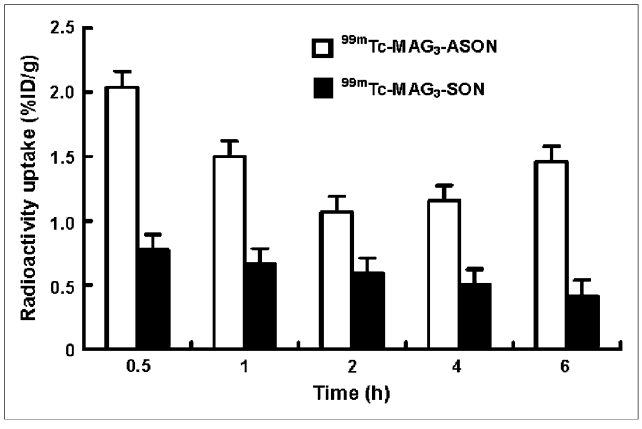

FIGURE 4. Radioactivity uptake in tumors after injection of ^{99m}Tc-MAG3-ASON or ^{99m}Tc-MAG3-SON. At all time phases, tumor radioactivity uptakes of ^{99m}Tc-MAG3-ASON are significantly higher ($P < 0.05$) than those of ^{99m}Tc-MAG3-SON. Data are expressed as mean ± SD ($n = 5$). Tumor uptake gradually increased from 2 to 6 h after injection of ^{99m}Tc-MAG3-ASON. However, a decreasing trend in tumor uptake was evident after injection of ^{99m}Tc-MAG3-SON.

One major problem of antisense technology is to improve the stability of oligonucleotides. To date, 3 generations of chemically modified oligonucleotides have been used, including phosphorothioate oligonucleotide, methylphosphonates, peptide nucleic acid (PNA), morpholino, and chimeric molecules (PNA/DNA-chimera). Although many analogs overcome the stability problem, the phosphorothioate modification, which has acceptable physical and chemical properties and shows reasonable resistance to nucleases, still represents the most widely used class of antisense compounds (*31*). Several pharmaceuticals based on it have been in clinical application or under clinical trails. We used uniformly phosphorothioate-modified oligonucleotide in this study and proved its specificity and stability in vitro when radiolabeled with ^{99m}Tc.

Another major obstacle for efficient antisense technology is the low internalization rate of oligonucleotides into target cells. There are no direct receptors in the cell membrane for oligonucleotides, so the uptake mechanism is nonspecific and relies on binding to cell-surface proteins or receptor-mediated adsorptive endocytosis or pinocytosis, which are known to be concentration and energy dependent (*29,32*). The other uptake mechanism is through a direct cell-membrane permeation process, which is more efficient (*31*). Depending on the oligonucleotides, cell line, and experimental conditions, the cell uptake rate ranges from 1% to 20% (*33*). Nowadays, transfection with liposomes, ligand-conjugated polyethyleneimine complex, and viral-derived agents (particularly adenoviruses and retroviruses)

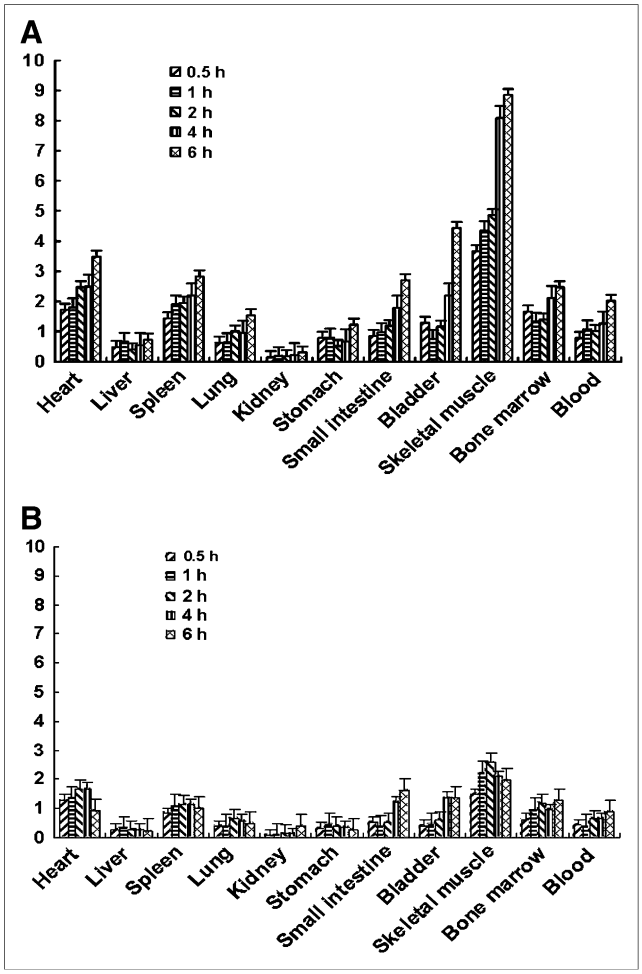

FIGURE 5. Tumor-to-organ ratios after injection of ^{99m}Tc-MAG3-ASON (A) or ^{99m}Tc-MAG3-SON (B) in tumor-bearing nude mice. Ratios were calculated from data of Tables 2 and 3. Data are expressed as mean ± SD (n = 5).

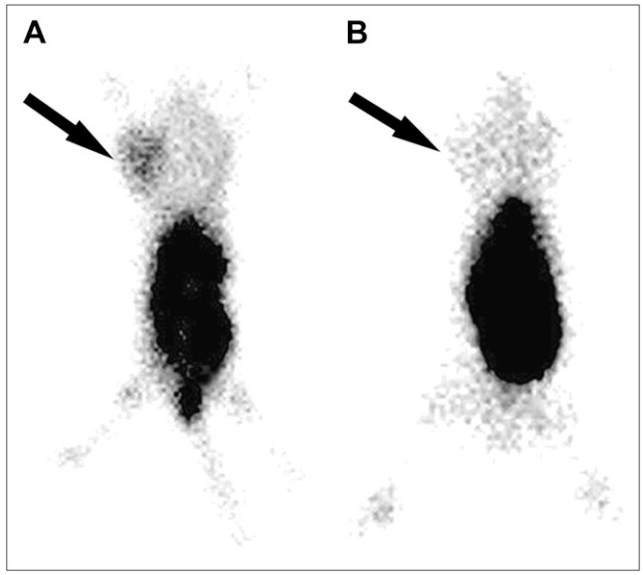

FIGURE 6. Imaging of hTERT expression in MCF-7 xenografts in BALB/c *nu/nu* mice using ^{99m}Tc-MAG3-ASON (A) or ^{99m}Tc-MAG3-SON (B). Planar γ-camera images were collected 6 h after administration of imaging probe. Tumor (arrow) is clearly visualized after injection of ^{99m}Tc-MAG3-ASON but is not clearly evident after injection of ^{99m}Tc-MAG3-SON.

have been applied in antisense technology (*34–36*). In vitro, liposomes or viral vectors are required to efficiently transfect cells with phosphorothioate ASONs, but transfection does not seem necessary in vivo, as the inhibition of the expression of the target can be accomplished with ASONs alone (*37*). Interestingly, in animal models and in patients, all therapeutically active ASONs have been administered in the form of naked compounds. It has been elucidated that in intact tissues other mechanisms exist, which can act in the same way as cationic carrier lipids (*31*). In the present study, we introduced the probes into cells using liposome. As for animal experiments, however, we injected the radiolabeled oligonucleotides directly.

The results of RT-PCR showed that in comparison with ^{99m}Tc-MAG3-SON, ^{99m}Tc-MAG3-ASON could inhibit the expression of hTERT mRNA significantly as well as ASON. It was proven that the antisense probe hybridized to the sequence on the whole hTERT mRNA in cells specifically and decreased the expression of hTERT mRNA. A reduction of hTERT transcript number after anti-hTERT ASON treatment was also observed by Zhang and He in leukemic cell lines (*16*) and Kraemer et al. in human bladder cancer cell lines (*30*).

The biodistribution of ^{99m}Tc-MAG3-ASON (and ^{99m}Tc-MAG3-SON) in mice bearing MCF-7 xenografts showed that the radiolabeled probes preferentially accumulated in the kidney and liver, and lesser accumulation was observed in the stomach, indicating the imaging agent was cleared primarily through the urinary system and digestion system. At any time points after injection, the accumulation of ^{99m}Tc-MAG3-ASON in the tumor tissue was significantly higher than that of ^{99m}Tc-MAG3-SON ($P < 0.05$). Furthermore, the accumulation of ^{99m}Tc-MAG3-ASON in the tumor tissue increased gradually from 2 until 6 h after injection, whereas that of ^{99m}Tc-MAG3-SON in tumor tissue decreased. We noted that the uptake curves between 2 and 6 h reflected the specific cellular retention, possibly related to the specific hybridization of the antisense probe on the targeted sequence. However, there was a relatively high uptake of ^{99m}Tc-MAG3-ASON/SON at 30 min and 1 h, because at the early times after injection, the measured radioactivity reflected the transport of the probe (*26*) and corresponded to a nonspecific phenomenon. As for the different uptake of the 2 probes at 30 min and 1 h, we proposed that this was related to cell-membrane nonspecific binding, which could reasonably be different, for physicochemical reasons, for the 2 different molecules. In addition, the ratios of T/NT after injection of ^{99m}Tc-MAG3-ASON were significantly higher than those after injection of ^{99m}Tc-MAG3-SON. These results could support the mechanism of antisense—that is, the specific hybridization of

^{99m}Tc-MAG3-ASON to hTERT mRNA results in the specific accumulation of radiolabeled ASON in the hTERT-expressed tumors.

A differential antisense accumulation in ACHN tumor cells (a human renal adenocarcinoma cell type) was visualized with microautoradiography (*12*), which demonstrated the intracellular localization of the tracers. As for in vivo imaging, further evidence concerning the reality of the intracellular localization of the tracers after intravenous injection should also be provided. For example, real-time PCR or immunohistochemistry can specifically measure the target mRNA or protein level after injection of antisense probe. Microautoradiography can find radioactivity inside cells if the specific retention really does correspond to the hybridization between antisense probe and targeted mRNA.

The results of imaging of hTERT expression in MCF-7 xenografts using the radiolabeled probes were consistent with the results of biodistribution. Tumors were clearly visualized after injection of ^{99m}Tc-MAG3-ASON but were not clearly imaged after injection of ^{99m}Tc-MAG3-SON. High uptake and retention in kidneys and liver is a general problem for radiometal-labeled oligonucleotides. This is also an apparent obstacle for imaging the tumors in these organs. However, this does not seem to be a problem for SPECT of hTERT expression in breast carcinomas in our study, where the tumor is anatomically well separated from the kidneys and liver.

All results of our study give a good reason that ^{99m}Tc-MAG3-ASON targeting hTERT mRNA can be used for detection of hTERT expression in malignant tumors in vivo. However, improvements in tumor delivery and normal tissue clearance are needed for further study on antisense imaging.

CONCLUSION

The expression of hTERT, a critical cancer hallmark, can be measured by ^{99m}Tc-MAG3-ASON targeting hTERT mRNA, which is a potential and promising candidate for visualization of hTERT expression in carcinomas.

ACKNOWLEDGMENTS

Professor Donald J. Hnatowich (University of Massachusetts Medical School) is kindly acknowledged for providing *S*-acetyl NHS-MAG3 for conjugation. This study was supported by grants from the National Natural Science Foundation of China (NSFC 30470498 and 30670583), the National Basic Research Program (973 Program, 2006CB705705-1), and the second phase of National Education Ministry 985 Project (985-2-056).

REFERENCES

1. Hanahan D, Weinberg RA. The hallmarks of cancer. *Cell.* 2000;100:57–70.
2. Beattie TL, Zhou W, Robinson MO, Harrington L. Reconstitution of human telomerase activity in vitro. *Curr Biol.* 1998;8:177–180.
3. Chang JT, Chen YL, Yang HT, Chen CY, Cheng AJ. Differential regulation of telomerase activity by six telomerase subunits. *Eur J Biochem.* 2002;269:3442–3450.
4. Wirth T, Kühnel F, Kubicka S. Telomerase-dependent gene therapy. *Curr Mol Med.* 2005;5:243–251.
5. Hiyama E, Hiyama K. Telomerase as tumor marker. *Cancer Lett.* 2003;194:221–233.
6. Lee KH, Rudolph KL, Ju YJ, et al. Telomere dysfunction alters the chemotherapeutic profile of transformed cells. *Proc Natl Acad Sci USA.* 2001;98:3381–3386.
7. Massoud TF, Gambhir SS. Molecular imaging in living subjects: seeing fundamental biological processes in a new light. *Genes Dev.* 2003;17:545–580.
8. Blasberg R. PET imaging of gene expression. *Eur J Cancer.* 2002;38:2137–2146.
9. Groot-Wassink T, Aboagye EO, Wang Y, Lemoine NR, Keith WN, Vassaux G. Noninvasive imaging of the transcriptional activities of human telomerase promoter fragments in mice. *Cancer Res.* 2004;64:4906–4911.
10. Padmanabhan P, Otero J, Ray P, et al. Visualization of telomerase reverse transcriptase (hTERT) promoter activity using a trimodality fusion reporter construct. *J Nucl Med.* 2006;47:270–277.
11. Saji H. Development of radiopharmaceuticals for molecular imaging. *Int Congr Ser.* 2004;1264:139–147.
12. Zhang YM, Wang Y, Liu N, Zhu ZH, Rusckowski M, Hnatowich DJ. In vitro investigations of tumor targeting with ^{99m}Tc-labeled antisense DNA. *J Nucl Med.* 2001;42:1660–1669.
13. Winnard P Jr, Chang F, Rusckowski M, Mardirossian G, Hnatowich DJ. Preparation and use of NHS-MAG_3 for technetium-99m labeling of DNA. *Nucl Med Biol.* 1997;24:425–432.
14. Poole JC, Andrews LG, Tollefsbol TO. Activity, function, and gene regulation of the catalytic subunit of telomerase (hTERT). *Gene.* 2001;269:1–12.
15. Orlando C, Gelmini S, Selli C, Pazzagli M. Telomerase in urological malignancy. *J Urol.* 2001;166:666–673.
16. Zhang Y, He DM. Effect of antisense hTERT mRNA oligodeoxynucleotide on telomerase activity of leukemic cells. *Cell Biol Int.* 2002;26:427–431.
17. Dewanjee MK, Ghafouripour AK, Kapadvanjwala M, et al. Noninvasive imaging of c-myc oncogene messenger RNA with indium-111-antisense probes in a mammary tumor-bearing mouse model. *J Nucl Med.* 1994;35:1054–1063.
18. Tian X, Aruva MR, Rao PS, et al. Imaging oncogene expression. *Ann NY Acad Sci.* 2003;1002:165–188.
19. Nakamura K, Kubo A, Hnatowich DJ. Antisense targeting of P-glycoprotein expression in tissue culture. *J Nucl Med.* 2005;46:509–513.
20. Tian X, Aruva MR, Qin W, et al. External imaging of CCND1 cancer gene activity in experimental human breast cancer xenografts with ^{99m}Tc-peptide-peptide nucleic acid-peptide chimeras. *J Nucl Med.* 2004;45:2070–2082.
21. Bai J, Yokoyama K, Kinuya S, et al. In vitro detection of mdr1 mRNA in murine leukemia cells with ^{111}In-labeled oligonucleotide. *Eur J Nucl Med Mol Imaging.* 2004;31:1523–1529.
22. Gallazzi F, Wang Y, Jia F, et al. Synthesis of radiometal-labeled and fluorescent cell-permeating peptide-PNA conjugates for targeting the bcl-2 proto-oncogene. *Bioconjug Chem.* 2003;14:1083–1095.
23. Lendvai G, Velikyan I, Bergström M, et al. Biodistribution of ^{68}Ga-labelled phosphodiester, phosphorothioate, and 2′-O-methyl phosphodiester oligonucleotides in normal rats. *Eur J Pharm Sci.* 2005;26:26–38.
24. Sun X, Fang H, Li X, Rossin R, Welch MJ, Taylor JS. MicroPET imaging of MCF-7 tumors in mice via unr mRNA-targeted peptide nucleic acids. *Bioconjug Chem.* 2005;16:294–305.
25. Wang RF, Shen J, Zhang CL, Liu M, Guo FQ. Study on biodistribution and imaging of radioiodinated antisense oligonucleotides in nude mice bearing human lymphoma [abstract]. *J Nucl Med.* 2006;47(5 suppl 2):428P.
26. Touboul M, Gauchez AS, D'Hardemare Adu M, et al. Early detection of chemoresistance in vivo through the use of a radiolabeled *antisense* oligonucleotide. *Anticancer Res.* 2002;22:3349–3356.
27. Vickers TA, Wyatt JR, Freier SM. Effects of RNA secondary structure on cellular antisense activity. *Nucleic Acids Res.* 2000;28:1340–1347.
28. Scherr M, Rossi JJ, Sczakiel G, Patzel V. RNA accessibility prediction: a theoretical approach is consistent with experimental studies in cell extracts. *Nucleic Acids Res.* 2000;28:2455–2461.
29. Gauchez AS, Du Moulinet D'Hardemare A, Lunardi J, Vuillez JP, Fagret D. Potential use of radiolabeled *antisense* oligonucleotides in oncology. *Anticancer Res.* 1999;19:4989–4997.
30. Kraemer K, Fuessel S, Schmidt U, et al. Antisense-mediated hTERT inhibition specifically reduces the growth of human bladder cancer cells. *Clin Cancer Res.* 2003;9:3794–3800.
31. Jansen B, Zangemeister-Wittke U. Antisense therapy for cancer: the time of truth. *Lancet Oncol.* 2002;3:672–683.

32. Britz-Cunningham SH, Adelstein SJ. Molecular targeting with radionuclides: state of the science. *J Nucl Med.* 2003;44:1945–1961.
33. Haberkorn U, Mier W, Eisenhut M. Scintigraphic imaging of gene expression and gene transfer. *Curr Med Chem.* 2005;12:779–794.
34. Dodds E, Dunckley MG, Naujoks K, Michaelis U, Dickson G. Lipofection of cultured mouse muscle cells: a direct comparison of lipofectamine and DOSPER. *Gene Ther.* 1998;5:542–551.
35. Schofield JP, Caskey CT. Non-viral approaches to gene therapy. *Br Med Bull.* 1995;51:56–71.
36. Hnatowich DJ, Nakamura K. Antisense targeting in cell culture with radiolabeled DNAs: a brief review of recent progress. *Ann Nucl Med.* 2004;18:363–368.
37. Gleave ME, Monia BP. Antisense therapy for cancer. *Nat Rev Cancer.* 2005;5:468–479.